Zinc(II)-Selective Ratiometric Fluorescent Sensors Based on Inhibition of Excited-State Intramolecular Proton Transfer

Maged M. Henary, Yonggang Wu, and Christoph J. Fahrni*[a]

Abstract: To develop a zinc(II)-selective emission ratiometric probe suitable for biological applications, we explored the cation-induced inhibition of excited-state intramolecular proton transfer (ESIPT) with a series of 2-(2′-benzenesulfonamidophenyl)benzimidazole derivatives. In the absence of Zn^{II} at neutral pH, the fluorophores undergo ESIPT to yield a highly Stokes' shifted emission from the proton-transfer tautomer. Coordination of Zn^{II} inhibits the ESIPT process and yields a significant hypsochromic shift of the fluorescence emission maximum. Whereas the paramagnetic metal cations Cu^{II}, Fe^{II}, Ni^{II}, Co^{II}, and Mn^{II} result in fluorescence quenching, the emission response is not altered by millimolar concentrations of Ca^{II} or Mg^{II}, rendering the sensors selective for Zn^{II} among all biologically important metal cations. Due to the modular architecture of the fluorophore, the Zn^{II} binding affinity can be readily tuned by implementing simple structural modifications. The synthesized probes are suitable to gauge free Zn^{II} concentrations in the micromolar to picomolar range under physiological conditions.

Keywords: fluorescent probes · ligand design · proton transfer · sensors · zinc

Introduction

The development of cation-selective fluorescence sensors has been an important goal of coordination chemistry for decades.[1] Fluorescence-based probes provide high sensitivity and are therefore particularly well suited for the visualization of metal cations in biological environments.[2] The majority of fluorescence sensors function as cation-responsive optical switches that translate the binding event into an increase or decrease of the emission intensity.[3] Due to the linear relationship between intensity and cation concentration, quantitative measurements are, in principle, possible; however, the emission intensity depends also on the sensor concentration, which is typically not known with sufficient accuracy in biological applications. Because the sensor enters the cell through passive diffusion across the plasma membrane, the intracellular concentration may vary as a function of incubation time, temperature, membrane permeability, and variations in cell size.

Ratiometric probes that exhibit a spectral shift upon binding of the cation offer an elegant solution to this problem. The ratio of the emission intensities at two excitation or emission wavelengths varies as a function of the cation concentration, but is independent of the probe concentration, pathlength, or spectral sensitivity of the instrument.[4] This approach was originally developed for the visualization of calcium-ion fluxes in live cells,[5] and a number of ratiometric sensors are now commercially available.[6] More recently, studies on various eukaryotic cell lines indicate the presence of intracellular compartments containing weakly bound, labile Zn^{II} (presumably up to millimolar concentrations). To study the dynamics of compartmentalized Zn^{II} in live cells quantitatively, a cell-permeable, emission ratiometric sensor would be very beneficial. Most of the currently available cell-permeable Zn^{II} probes function only as fluorescence switches and are not suitable for ratiometric measurements.[17–22] Furthermore, due to the high cost of laser equipment, modern 3D-imaging tools, such as confocal and multiphoton microscopy, depend on a single-excitation light source. To take advantage of these new imaging techniques, the sensor must provide a spectral shift of the peak emission; however, with the exception of IndoZin,[23] currently available cell-permeable ratiometric Zn^{II} sensors require dual excitation and are therefore not suitable for these applications.[6,23,24,52]

To develop a Zn^{II}-selective emission ratiometric probe, we recently explored the photophysics of cation-induced inhibition of excited-state intramolecular proton transfer (ESIPT).[25] Benzimidazole derivatives (T_A) containing an intramolecular hydrogen bond undergo ESIPT and yield a highly Stokes' shifted emission from the proton-transfer tautomer T_B^* (Scheme 1).[26–30] If the acidity of the proton at-

[a] Dr. M. M. Henary, Y. Wu, Prof. Dr. C. J. Fahrni
School of Chemistry and Biochemistry
Georgia Institute of Technology
770 State Street, Atlanta, GA 30332 (U.S.A.)
Fax: (+1) 404-894-2295
E-mail: fahrni@chemistry.gatech.edu

 DOI: 10.1002/chem.200305299

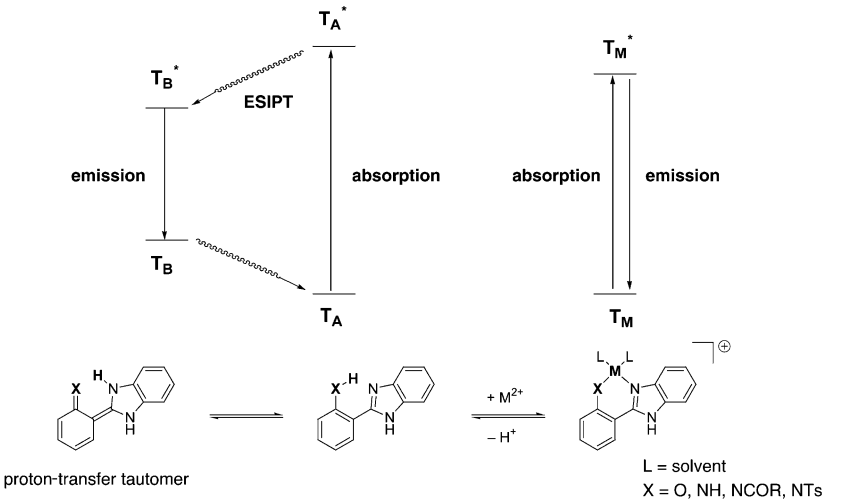

Scheme 1. Simplified Jablonski diagram illustrating the increase of the emission energy upon metal-cation-induced inhibition of excited-state intramolecular proton transfer.

tached to X is sufficiently high, coordination of a metal cation M^{2+} will remove this proton and disrupt the ESIPT process. Since emission of the coordinated species TM* occurs with normal Stokes' shift, a significant blueshift is expected. For example, the acidity of the phenol proton in 2-(2′-hydroxyphenyl)benzimidazole (**I**) is sufficiently high, such that Zn^{II} coordination in organic solvents does indeed yield the expected blueshift of the peak emission.[25]

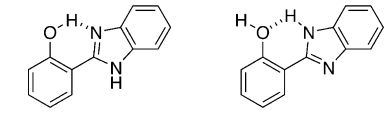

I (cis) **I** (trans)

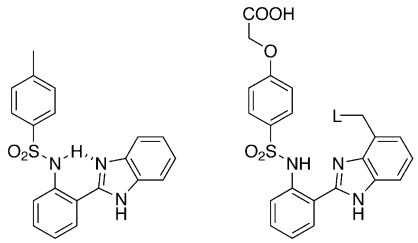

II **III**

However, in aqueous solution the proton-transfer emission of 2-(2′-hydroxyphenyl)benzimidazole is surprisingly weak, and the spectrum is dominated by a normal emission band, which presumably originates from the *trans*-rotamer that cannot undergo ESIPT.[25,28] In contrast, 2-(2′-tosylaminophenyl)benzimidazole (**II**) lacks the electron lone pair required to stabilize the *trans*-rotamer by means of intramolecular hydrogen bonding. With only the *cis*-rotamer present, both in organic solvents and aqueous solution, the molecule exclusively exhibits the emission of the ESIPT tautomer with a large quantum yield (0.3–0.5).[31] Given the similar acidity of sulfonamides and phenols, coordination of Zn^{II} should also result in displacement of the proton and inhibition of the ESIPT process as observed for the phenol derivative **I**. Hence, to evaluate this fluorophore as a platform for the design of Zn^{II}-selective ratiometric probes, we synthesized a family of water soluble 2-(2′-benzenesulfonamidophenyl)benzimidazole derivatives (**III**) and studied their emission responses towards biologically important metal cations under physiological conditions. Furthermore, to explore the tunability of the Zn^{II} affinity and selectivity, we introduced various Lewis base donors (L) in proximity to the bidentate cation binding site.

Results and Discussion

Synthesis: By using a modular approach, ligands **7**–**9** were synthesized from precursor **5** (Scheme 2). Coupling of commercially available amine **1** with sulfonyl chloride **2**,[32] followed by oxidation of the benzylic hydroxyl group with manganese(IV) oxide provided aldehyde **3**. Copper(II)-mediated coupling with 1,2-diamino-3-hydroxymethylbenzene[33] (**4**) followed by oxidation with manganese(IV) oxide gave key intermediate **5**, which was readily converted to the substituted ligands **7a**, **8a**, and **9a** by means of reductive amination with the corresponding amines. The unsubstituted derivative **6a** is principally accessible by oxidative coupling of **3** with 1,2-phenylenediamine; however, since 2-(2′-aminophenyl)benzimidazole is commercially available, ligand **6a** is better synthesized through condensation with sulfonyl chloride **2** in a single step. The water-soluble acids **6b**, **7b**, **8b**, and **9b** were obtained by hydrolysis with lithium hydroxide in aqueous methanol.

Protonation equilibria: The protonation equilibria of the four benzimidazole ligands **6b**, **7b**, **8b**, and **9b** were investigated by potentiometric and spectrophotometric titrations. For the determination of the pK_a values, a solution of each ligand in water (0.5–1 mM) was titrated with 0.1 M KOH at a constant ionic strength of 0.1 M KCl (Figure 1). The measured potential data were converted to $-\log[H_3O^+]$ based on the electrode potential (E_0) and slope s, which were determined by Gran's method;[34] nonlinear least-squares fit analysis[35] provided the corresponding pK_a values (Table 1).

Ligand **6b** exhibits two protonation steps with $pK_a = 8.0$ and 4.5, which can be readily assigned to the nitrogen atom of sulfonamide and the carboxylic acid moiety, respectively. The tertiary-amine substituent in ligand **7b** yields an addi-

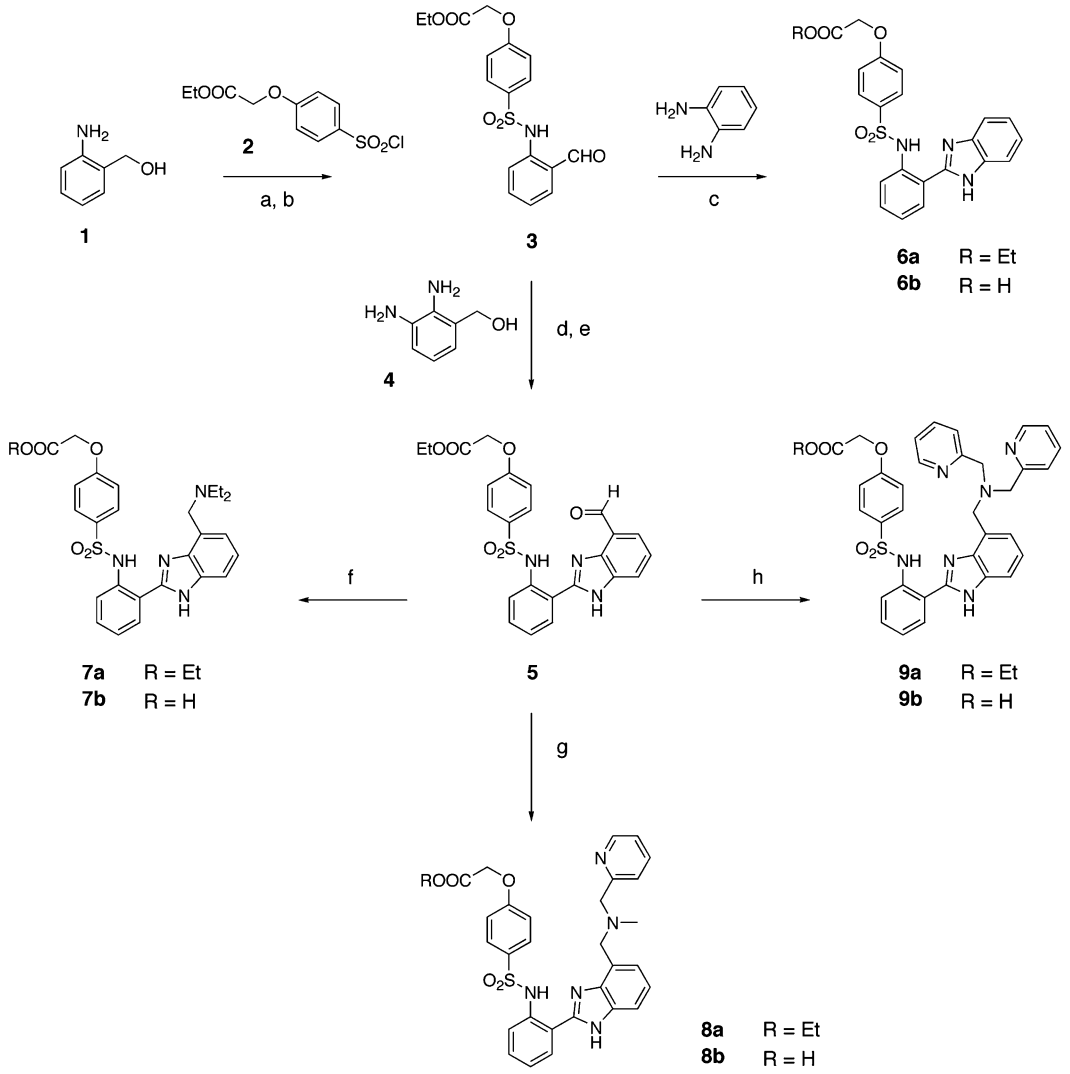

Scheme 2. a) pyridine, 0 °C; b) MnO_2, CH_2Cl_2, RT (53 %, from **1**); c) $Cu(OAc)_2$, EtOH, reflux (20 %); d) $Cu(OAc)_2$, EtOH, reflux (36 %); e) MnO_2, CH_2Cl_2, RT (86 %); f) $NaBH(OAc)_3$, Et_2NH, 1,2-$EtCl_2$ (76 %); g) $NaBH(OAc)_3$, *N*-2-picolyl-*N*-methylamine, 1,2-$EtCl_2$ (97 %); h) $NaBH(OAc)_3$, *N*,*N*-2,2′-dipicolylamine, 1,2-$EtCl_2$ (80 %).

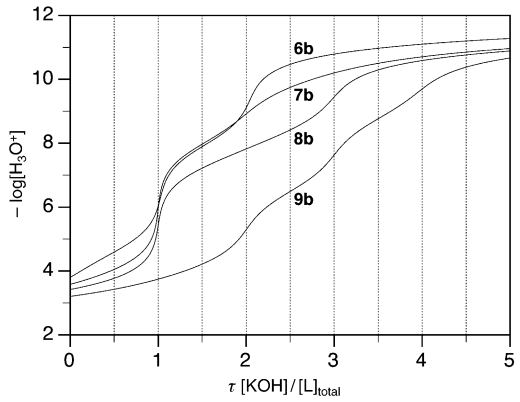

Figure 1. Potentiometric titration curves for ligands **6b**–**9b** in water (0.1 M KCl, 25 °C; ligand concentrations (mM): **6b** 1.0; **7b** 0.47; **8b** 0.64; **9b** 0.76).

tional protonation step with $pK_a = 10.1$. Consistent with the presence of an ammonium cation, protonation of the carboxylic acid moiety now requires more acidic conditions ($pK_a = 3.73$) compared with **6b**. The picolyl susbtituents in **8b** and **9b** substantially lower the pK_a of the nitrogen atom of the tertiary amine, an observation which is in agreement with the reported low pK_a (7.3) of bispicolylamine.[36,37] Because protonation of the nitrogen atom of sulfonamide is expected to occur in the same pH range, the pK_a assignment to either functional group is ambiguous for **8b** and **9b**.

To clarify this ambiguity we performed additional spectrophotometric titrations. The spectral changes associated with deprotonation of the nitrogen atom of sulfonamide provide a characteristic signature to unequivocally assign the corresponding pK_a values. Deconvolution analysis of the UV-visible traces with the SPECFIT software package[38] provided the absorption spectra for the species with protonated and deprotonated sulfonamide nitrogen atoms (Figure 2, left). The absorption maxima of the deconvoluted spectra are included in Table 1 for ligands **6b**, **7b**, **8b**, and **9b**. Hence, for both ligands **8b** and **9b** the highest pK_a values correspond to protonation of the nitrogen atom of sulfonamide, while the next lowest pK_a values are associated with the picolyl-

Table 1. Protonation constants and photophysical data for ligands **6b**, **7b**, **8b**, and **9b** in aqueous solution.[a]

Species/Equilibrium	Data	**6b**	**7b**	**8b**	**9b**
$[LH^-]/[H^+][L^{2-}]$	pK_1	8.04 ± 0.03	10.12 ± 0.03	8.42 ± 0.03	8.73 ± 0.03
$[LH_2]/[H^+][LH^-]$	pK_2	4.50 ± 0.03	8.02 ± 0.03	7.31 ± 0.03	6.49 ± 0.03
$[LH_3^+]/[H^+][LH_2]$	pK_3	n/a	3.73 ± 0.05	3.33 ± 0.05	4.05 ± 0.03
$[LH_4^{2+}]/[H^+][LH_3^+]$	pK_4	n/a	n/a	n/a	2.84 ± 0.05
L^{2-}	absorption λ_{max} [nm][b]	301 (15870)	304 (10120)[f]	303(15170)	304 (12320)
		329 (10920)	326 (7470)[f]	329 (10600)	332 (9220)
	excitation λ_{max} [nm][c]	296	299[f]	297	297
	emmission λ_{max} [nm][c]	418	419[f]	419	419
	Stokes' shift [cm^{-1}]	6470	6810[f]	6530	6250
LH^-	absorption λ_{max} [nm][b]	299 (12300)	306 (9360)[g]	305 (12850)	305 (10100)
	excitation λ_{max} [nm][d]	300	309[g]	309	308
	emission λ_{max} [nm][d]	460	469[g]	471	460
	Stokes' shift [cm^{-1}]	11700	11360[g]	11550	11050
	quantum yield[e]	0.23	0.32[g]	0.28	0.09

[a] 0.1 M KCl, 25°C; [b] From deconvolution analysis, molar extinction coefficient [$L\,mol^{-1}\,cm^{-1}$] in parentheses; [c] pH 11.0, 0.1 M KCl; [d] pH 7.00, 10 mM PIPES, 0.1 M KCl; [e] Quinine sulfate in 1 N H_2SO_4 as standard; [f] Monoprotonated species LH^-; [g] Diprotonated species LH_2.

amine substituents. In summary, deprotonation of the sulfonamide moiety occurs for all ligands at $-\log[H_3O^+] > 8$ and yields qualitatively identical absorption spectra with a sharp peak around 300 nm and a red-shifted band centered around 330 nm (Figure 2, left). The substituents attached to the benzimidazole ring in ligand **7b**, **8b**, and **9b** are electronically decoupled from the chromophoric π-system and consequently show no significant influence on the absorption spectra. As illustrated by the distribution diagram in Figure 3, the protonated sulfonamide species

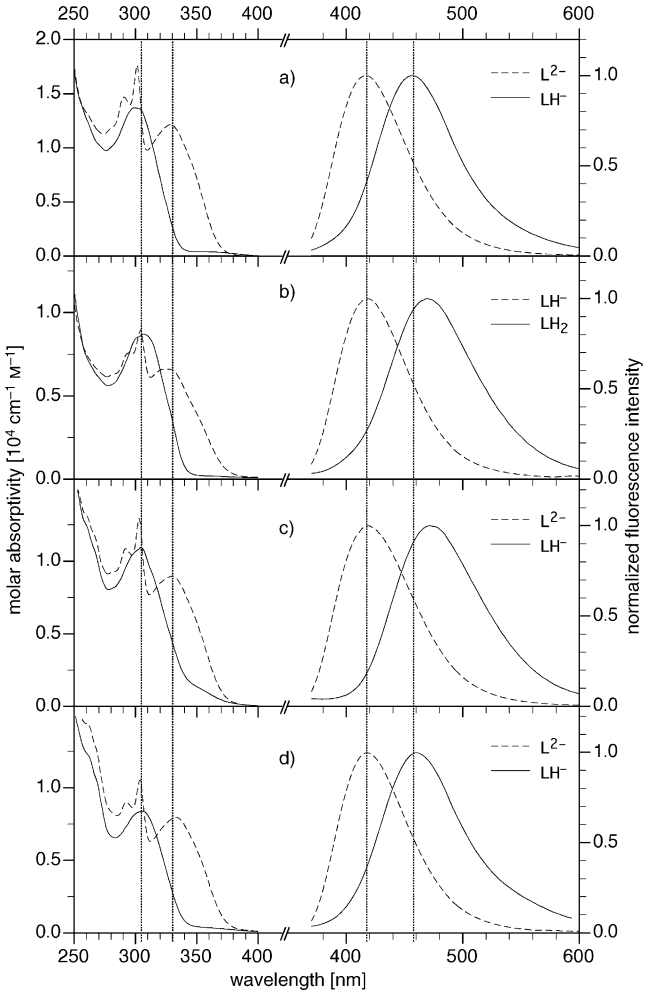

Figure 2. Comparison of the UV-visible absorption (left) and normalized fluorescence emission spectra (right) of the species with protonated (——) and deprotonated (– – –) sulfonamide nitrogen atom in aqueous solution (0.1 M KCl, 25°C) for ligands a) **6b**, b) **7b**, c) **8b**, and d) **9b**. The emission spectra were recorded at pH 7.2 (——) and 11.0 (– – –). The UV-visible traces were obtained through deconvolution of a series of spectra with pH range 7–10.

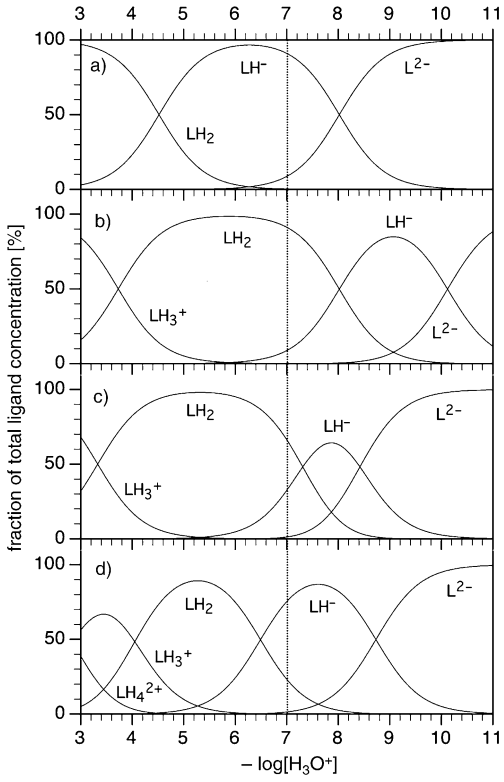

Figure 3. Calculated species distribution diagrams for ligands a) **6b**, b) **7b**, c) **8b**, and d) **9b**.

dominate the equilibrium composition at neutral pH. However, the lower protonation constants of ligands **6b** and **7b** are responsible for the presence of approximately 10% of the sulfonamide anion, thus shifting the optimal conditions for ratiometric cation measurements for these two ligands to a lower pH range.

Upon excitation at the peak-absorption wavelength, all four ligands **6b**–**9b** display an intense fluorescence emission with a quantum yield range of 9–32%. At neutral pH, the

emission spectrum of each ligand consists of a single band centered uniformly around 460 nm (Figure 2, right). The spectra are not influenced by the choice of excitation wavelength, suggesting the presence of a single, emissive species in the excited-state manifold. The large Stokes' shifts, averaging approximately 11 000 cm^{-1}, are characteristic for emission of the corresponding proton-transfer tautomer T_B^*.[31] Deprotonation of the nitrogen atom of sulfonamide disrupts the ESIPT process and results in a blueshifted, normal emission band of the sulfonamide anion around 419 nm. Unlike the structurally related 2-(2′-hydroxyphenyl)benzimidazoles, which exhibit multiple emission bands under identical conditions,[22,28] ligands **6b–9b** display uniform photophysical properties, which render them potentially suitable as cation-selective probes.

Ground-state tautomerism: The NH-proton in benzimidazoles is known to undergo rapid, annular tautomerization.[39] While in the case of ligands **6a/b** the annular tautomerization corresponds to a degenerate equilibrium, the tautomer pairs of the substituted ligands **7a/b–9a/b** are structurally different and represent a nondegenerate, prototropic equilibrium (Scheme 3). The ^{1}H NMR spectra of ligands **6a/b–9a/b** all contain a single set of resonances for the benzimidazole protons. Conclusively, the tautomerization rate at room temperature is too fast to be observed on the NMR timescale, resulting in a spectrum at the fast-exchange limit with averaged signals. As exemplified by ligand **7a** in CD_3OD, at lower temperatures the proton resonances undergo line broadening (Figure 4); however, even at −60 °C the tautomerization rate does not reach the slow-exchange limit that would provide the chemical-shift information for each tautomer and their concentration ratio. The data set is therefore not suitable to determine the equilibrium constant and activation barrier of the prototropic equilibrium.

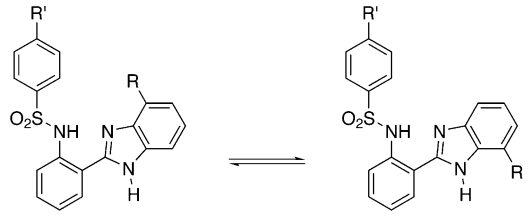

Scheme 3. Nondegenerate prototropic equilibrium of the tautomer pairs of the substituted ligands **7a/b–9a/b**.

The tautomerization equilibrium constants for 4(7)-substituted benzimidazoles reported in the literature are very close to 1, indicating near equivalence in the stability of the N1(H) and N3(H) tautomers.[40] Thus, the stability difference between the annular tautomers of ligands **6–9** is primarily controlled by steric factors and presumably rather small. We therefore assume that both tautomers are present in significant concentrations, and that the previously discussed absorption and emission spectra correspond to the averaged spectra of both tautomers.

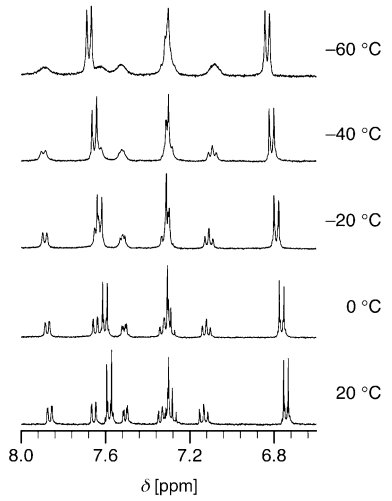

Figure 4. Variable-temperature ^{1}H NMR spectra of ligand **7a** in CD_3OD (3 mM).

Complexation studies: Among the biologically important metal cations, only Zn^{II} yielded a bright, blueshifted fluorescence emission when added to an aqueous solution of any of the four ligands **6b–9b**. At neutral pH, coordination of Ca^{II} and Mg^{II} is presumably too weak to replace the sulfonamide proton, and gives no visible change of the fluorescence emission. The paramagnetic transition-metal cations Mn^{II}, Co^{II}, Fe^{II}, Ni^{II}, and Cu^{II} coordinate to the ligands, but partially or completely quench the fluorescence emission. Given the selective fluorescence response towards Zn^{II}, we investigated the interaction of this cation with each of the four ligands **6b–9b** in more detail. A compilation of all thermodynamic and photophysical data obtained from these studies is given in Table 2.

Table 2. Thermodynamic and photophysical data for the complexation of ligands **6b–9b** with Zn^{II} in aqueous solution.[a]

Data	**6b**	**7b**	**8b**	**9b**
$\log K$[b]	4.50 ± 0.04	3.09 ± 0.04	9.23 ± 0.04	12.10 ± 0.04
absorption λ_{max} [nm][c]	327	318	297	334
excitation λ_{max} [nm]	294	299	300	338
emission λ_{max} [nm]	406	420	415	406
Stokes' shift [cm^{-1}]	5950	7640	9570	5310
R_{min} $F(400/500)$[d]	0.44	0.15	0.24	0.14
R_{max} $F(400/500)$[d]	8.46	3.06	7.34	11.6
R_{max}/R_{min}	19	20	30	82
quantum yield[e]	0.22	0.23	0.17	0.21

[a] 0.1 M $KClO_4$, 25 °C, 10 mM PIPES, pH 7.20; [b] Apparent binding constant at pH 7.20; [c] From deconvolution analysis; [d] Ratio R of fluorescence emission intensities at 400 and 500 nm; [e] Quinine sulfate in 1 N H_2SO_4 as standard.

Absorption and emission spectra: Since coordination to the sulfonamide group is accompanied by loss of the nitrogen-bound proton, the UV-visible spectrum should display a similar redshift as previously observed for the deprotonated sulfonamide anion (Figure 2). Addition of Zn^{II} triflate to ligand **6b** at neutral pH did indeed yield a new redshifted band at 327 nm and a single isosbestic point at 318 nm (Fig-

ure 5a, left). When excited at this wavelength, the emission spectra at various Zn^{II} concentrations also revealed an isosbestic point at 428 nm (Figure 5a, right), which is consistent with a simple equilibrium system involving free and Zn^{II}-bound ligands. As expected, displacement of the sulfonamide proton by Zn^{II} inhibits the ESIPT process and results in a significant blueshift of the peak emission.

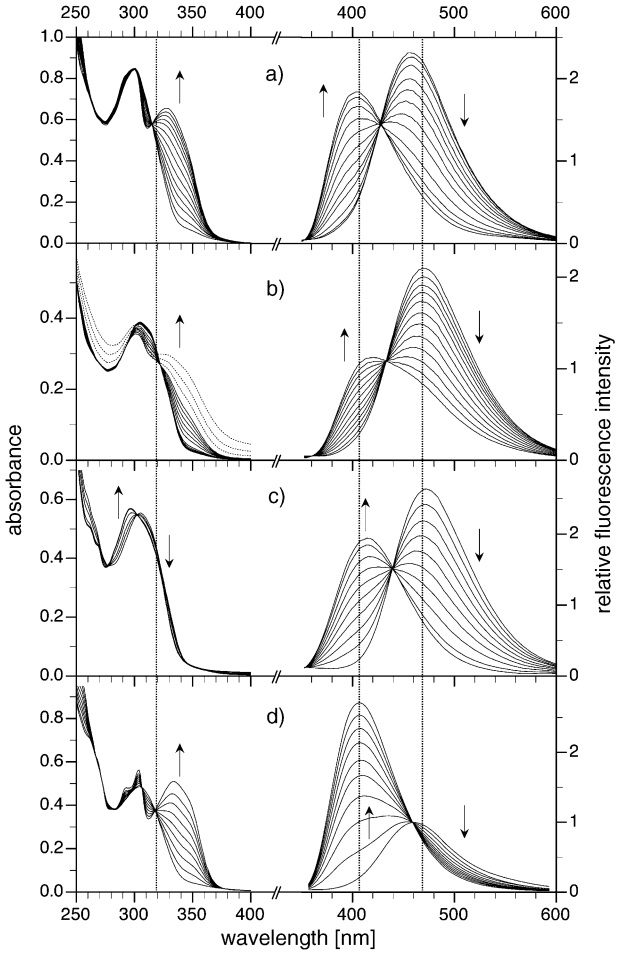

Figure 5. UV-visible absorbance (left) and fluorescence emission spectra (right) of ligands a) **6b**, b) **7b**, c) **8b**, and d) **9b** as a function of added Zn^{II} (excitation at the isosbestic point of the UV-visible traces, pH 7.20, 10 mM PIPES, 0.1 M $KClO_4$).

Ligand **7b** shows qualitatively the same behavior as **6b** (Figure 5b); however, at Zn^{II} concentrations above 10 mM the isosbestic point of the initial set of UV-visible traces is no longer conserved, indicating the formation of a new species (Figure 5b, left, dotted curves). The continuous increase of the absorbance over the entire wavelength range contradicts the presence of a stoichiometrically well-defined complex; this is possibly a result of precipitation and/or the formation of a coordination polymer.

In contrast, the UV-visible titration of ligand **8b** with Zn^{II} did not yield the expected redshifted absorption band as observed for **6b** and **7b** under identical conditions (Figure 5c, left). Evidently, the sulfonamide nitrogen atom does not participate in coordination to Zn^{II}, and remains protonated throughout the titration. Interestingly, the emission spectra acquired under identical conditions revealed the same characteristic blueshift as observed for **6b** and **7b**, and indicated inhibition of the ESIPT process. This might initially appear as a contradiction, however, the formation of the ESIPT tautomer requires not only the presence of the sulfonamide proton but also the proton-accepting electron lone pair of the benzimidazole nitrogen atom. If this nitrogen atom is coordinated to Zn^{II}, the ESIPT process is inhibited regardless of the protonation state of the sulfonamide group. This interpretation is further supported by the apparent Zn^{II} binding affinity of $\log K = 9.2$ (vide infra), which is significantly higher than the apparent binding affinity of the picolylamine moiety ($\log K_{Zn} = 3.1$, pH 7.2).[41]

Titration of ligand **9b** with Zn^{II} displayed a similar redshifted absorption band in the UV-visible spectrum as previously observed for **6b** and **7b**, indicating coordination of Zn^{II} to the sulfonamide nitrogen atom (Figure 5d, left). The high apparent binding affinity of $\log K = 12.1$ at neutral pH (vide infra) suggests formation of a pentadentate complex involving coordination of all five nitrogen-donor atoms. This assumption is additionally supported by a comparison with the apparent Zn^{II} affinity of dipicolylamine ($\log K_{Zn} = 7.3$ at pH 7.2),[41] which is five orders of magnitude lower than the affinity of **9b**. The fluorescence emission maxima again undergo a blueshift (Figure 5d, right), which is in agreement with the inhibition of ESIPT in favor of the normal emission of the Zn^{II}-bound fluorophore.

Apparent Zn^{II} binding affinities: The binding affinities at neutral pH of the four ligands **6b**–**9b** were determined by using nonlinear least-squares fit analysis of the emission responses at various Zn^{II} concentrations (Table 2). For ligands **6b** and **7b** the Zn^{II} affinities were directly obtained from mol–ratio plots with Zn^{II} concentrations ranging between 10 μM and 50 mM. The two ligands (**6b**, **7b**) bind Zn^{II} with $\log K = 4.50 \pm 0.04$ and 3.09 ± 0.04, respectively, and form both complexes with a 1:1 stoichiometry. Much to our surprise, the diethylamino substituent attached to the benzimidazole ring in **7b** did not yield an increase, but rather a decrease in binding affinity. Since the UV-visible traces indicate that the sulfonamide nitrogen atom is coordinated to Zn^{II}, it appears unlikely that the diethylamino group is also involved in complexation to the metal center. Compared with **8b** and **9b**, the nitrogen atom of the tertiary amine in **7b** is approximately three orders of magnitude more basic, and presumably remains protonated even in the presence of millimolar concentrations of Zn^{II}. The additional charge of the resulting ammonium cation might therefore be responsible for the unexpectedly low Zn^{II} affinity of **7b**.

Initial mol–ratio plots of the emission response of ligands **8b** and **9b** with Zn^{II} revealed a fractional saturation of $>99\%$ throughout the entire titration range, indicating a significantly higher binding affinity compared with **6b** or **7b**. Thus, to reliably measure the Zn^{II} affinity of $\log K = 9.23 \pm 0.04$ for **8b** a set of Zn^{II}/EGTA (EGTA = ethylenebis(oxyethylenenitrilo)tetraacetic acid) buffer solutions were used with free Zn^{II} concentrations ranging between 10 pM and 18 nM. Similarly, the affinity of $\log K = 12.10 \pm 0.04$ for **9b**

was determined with a set of Zn^{II}/HEDTA (HEDTA = *N*-(2-hydroxyethyl)ethylenediaminetriacetic acid) buffer solutions with free Zn^{II} ranging between 0.16–13 pM.

Ratiometric measurements: If the peak excitation or emission wavelengths are shifted upon binding of the metal cation, the ratio R of the intensities at two different wavelengths λ_1 and λ_2 is sufficient to determine the metal concentration, regardless of the probe concentration, path length, or other instrument-related parameters.[4] With a 1:1 binding stoichiometry the Zn^{II} concentration is given by Equation (1):

$$[Zn^{II}] = K_d\left(\frac{R-R_{min}}{R_{max}-R}\right)\frac{S_{apo}}{S_{bnd}} \quad (1)$$

in which R_{min} and R_{max} are the limiting R values in the absence and at saturating levels of Zn^{II}, respectively. The two instrument-specific factors S_{apo} and S_{bnd} are determined from solutions containing accurately known concentrations of the probe and Zn^{II}. Since R_{max}/R_{min} reflects the limiting dynamic range and resolution for concentration measurements, this parameter is a good measure to compare the performance of various probes. For each of the four ligands **6b**–**9b**, the ratio of the emission intensities at 400 and 500 nm were determined at various Zn^{II} concentrations covering at least one logarithmic unit above and below the corresponding dissociation constants. Nonlinear least-squares fit analysis using Equation (1) yielded the R_{min} and R_{max} values listed in Table 2. The calculated R_{max}/R_{min} ratios range between 19–82 and compare well to the commercially available ratiometric calcium probes indo-1 ($R_{max}/R_{min}=21$) or fura-2 ($R_{max}/R_{min}=45$).[4] A plot of the emission–intensity ratio versus the free Zn^{II} concentration further illustrates the dynamic range of each of the ligands **6b**–**9b** (Figure 6). For a better comparison, R_{max}/R_{min} was normalized to unity and the experimental ratios R were scaled accordingly. Because reliable concentration measurements are only feasible between 20–80% fractional saturation,[42] the analytically useful concentration range is typically restricted to one order of magnitude above and below the dissociation constant of the probe. Fluorophore **6b** is thus suitable to gauge free Zn^{II} between 30 μM and 3 mM, whereas the high-affinity probes **8b** and **9b** can be used for concentrations between 1–10 nM and 0.2–20 pM,

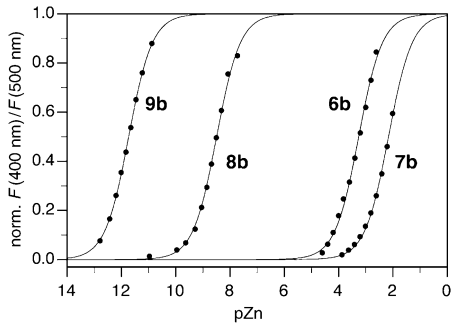

Figure 6. Change of the emission intensity ratio at 400 and 500 nm ($\lambda_{ex}=$ 320 nm) for ligands **6b**–**9b** as a function of free Zn^{II} ($pZn=-\log[Zn^{II}_{free}]$, pH 7.2, 10 mM PIPES, 0.1 M $KClO_4$).

respectively. The lower affinity of ligand **7b** does not significantly expand the dynamic range relative to **6b**, since according to the previously discussed UV-visible data, the binding stoichiometry is not conserved at Zn^{II} concentrations above 10 mM (see absorption and emission spectra section). This ligand was therefore excluded from the investigation of the emission response towards other biologically important metal cations.

Selectivity towards Zn^{II}: In coordination studies with other biologically relevant metal cations, ligands **6b**, **8b**, and **9b** revealed a selective response towards Zn^{II}. Since coordination of Zn^{II} results in a blueshift of the emission maximum to 405 nm, the emission intensity at this wavelength is a good indicator for the selectivity of the probe response (Figure 7). With up to millimolar concentrations of Ca^{II} and

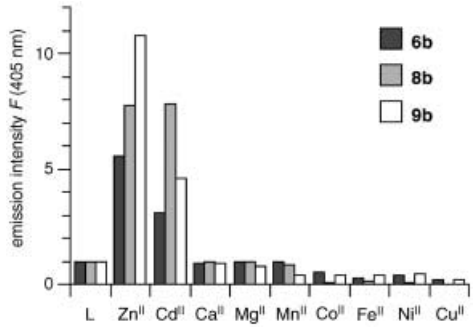

Figure 7. Emission intensity at 405 nm ($\lambda_{ex}=320$ nm) of ligands **6b**, **8b**, and **9b** in response to various metal cations. Concentrations: **6b** 10 μM, all M^{2+} 1 mM; **8b** 10 μM, Ca^{II}, Mg^{II} 1 mM, all other M^{2+} 10 μM; **9b** 10 μM, Ca^{II}, Mg^{II} 1 mM, all other M^{2+} 10 μM (pH 7.2, 10 mM PIPES, 0.1 M $KClO_4$).

Mg^{II} the emission spectra of all three ligands essentially remained unchanged, whereas the paramagnetic metal cations Cu^{II}, Fe^{II}, Ni^{II}, Co^{II}, and Mn^{II} resulted in fluorescence quenching. We also investigated the emission response for Cd^{II}: a nonbiological d^{10} metal cation that often exhibits similar coordination properties to Zn^{II}. In the presence of Cd^{II} all three ligands showed increased emission intensities at 405 nm; however, only **8b** yielded a similarly strong fluorescence enhancement as observed with Zn^{II} (Figure 7).

Figure 8 shows the emission intensity ratios at 400 and 500 nm as a function of selected divalent metal cations (dark columns). With the exception of Cu^{II}, the emission response of **6b** was not significantly altered by millimolar concentrations of the tested cations. The ligands **8b** and **9b** revealed a similar trend; however, Co^{II}, Ni^{II}, and Fe^{II} also yielded an increased emission ratio. Nevertheless, because the fluorescence emission in the presence of these cations is very weak, it should be possible to distinguish this ratio increase from the Zn^{II}-selective emission change (Figure 7).

To further gauge the selectivity of the ligands, the emission response of each cation was measured in the presence of an equimolar amount of Zn^{II} (Figure 8, light columns). Under these conditions the emission ratios for **8b** and **9b** were essentially restored to the same values as those observed for the Zn^{II}-saturated probe. Only the measurements

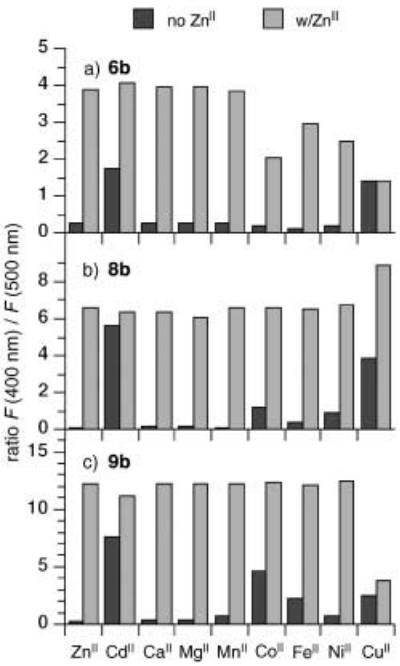

Figure 8. Emission intensity ratios at 400 and 500 nm in response to various metal cations (pH 7.2, 10 mM PIPES, 0.1 M $KClO_4$): a) 10 μM **6b**, all M^{2+} 1 mM; b) 10 μM **8b**, Ca^{II}, Mg^{II} 1 mM, all other M^{2+} 10 μM; c) 10 μM solution of **9b**, Ca^{II}, Mg^{II} 1 mM, all other M^{2+} 10 μM. Binding competition measurements were acquired after equilibration for 3 h (**6b**) and 24 h (**8b** and **9b**) with solutions containing equimolar concentrations of Zn^{II} and the respective metal cation.

with Cu^{II} resulted in a significant change in the emission ratio, but again induced fluorescence quenching. In comparison, the response of ligand **6b**, which is lacking any additional coordinating pyridine groups, was less selective. Whereas Ca^{II}, Mg^{II}, and Mn^{II} did not interfere with Zn^{II} binding, the emission ratios for Co^{II}, Fe^{II}, Ni^{II}, and Cu^{II} were significantly lower suggesting competitive binding of these cations; however, for Cd^{II}-induced fluorescence enhancements the emission ratios were essentially restored in the competition assays with all three ligands, indicating a lower binding affinity of Cd^{II} compared with Zn^{II}.

Conclusion

In summary, the benzimidazole derivatives **6b–9b** demonstrate that cation-induced inhibition of ESIPT leads to a substantial spectral shift of the fluorescence emission and is a promising concept for the development of Zn^{II}-selective ratiometric probes. The modular architecture of the probe principally allows for tuning of the binding affinity as illustrated with the picolylamine-substituted derivatives **8b** and **9b**. Because the spectral characteristics are not significantly altered by the attached substituents, the approach is suitable for generating a family of probes that can be used with a single filter set. Probes **6b–9b** require excitation in the UV range, which is a limiting factor for fluorescence microscopy applications. However, the probes can be used in any cuvette-based application, for example, in competition experiments for the determination of the binding affinities of spectroscopically silent ligands. The high-affinity probes **8b** and **9b** should be particularly suitable for the measurement of the binding affinities of Zn^{II} metalloproteins, whose binding constant is typically in the range between 10^8–$10^{12}\,M^{-1}$ (e.g., alkaline phosphatase, $K_{Zn}=10^7$–10^8,[43] carboxy peptidase, $K_{Zn}=2.1\times10^8$,[44] carbonic anhydrase, $K_{Zn}=1.3\times10^{12}$[45]). We anticipate that simple structural modifications through introduction of suitable substituents should yield a sufficiently redshifted excitation maximum and also render the fluorophore platform suitable for microscopy applications. To evaluate their suitability as Zn^{II}-selective probes in multiphoton laser microscopy, we are currently exploring the two-photon cross sections of these fluorophores. This approach would be particularly attractive for in vivo applications, since the required excitation wavelength corresponds to one-half of the single-photon energy.

Experimental Section

Materials and reagents: 2-Aminobenzyl alcohol (Aldrich, 98%), 2-(2′-aminophenyl)benzimidazole (Alfa-Aesar, 98%), phenol (Aldrich, 99%), ethyl bromoacetate (Aldrich, 98%), manganese dioxide (Aldrich, 99%), 1,2-phenylenediamine (Aldrich, 99%), copper acetate monohydrate (Aldrich, 98%), thionyl chloride (Aldrich, 99%), 2,2′-dipicolylamine (TCI, 97%), *N*,*N*-diisopropylethyl amine (Aldrich, 99%), *N*-(2-hydroxyethyl)-ethylenediaminetriacetic acid (HEDTA, Aldrich, 99%), ethylenebis(oxyethylenenitrilo)tetraacetic acid (EGTA, Aldrich, 97%). NMR: δ in ppm versus $SiMe_4$ (0 ppm, ^1H, 400 MHz). MS: selected peaks; *m*/*z*. Melting points are uncorrected. Flash chromatography: Merck silica gel (240–400 mesh). TLC: 0.25 mm, Merck silica gel 60 F_{254}, visualizing at 254 nm or with 2% $KMnO_4$ solution.

Synthesis: 2,3-Diaminobenzyl alcohol[33] **4** and ethyl 2-phenoxyacetate[46] were synthesized following the published procedures.

Ethyl (4-chlorosulfonylphenoxy)acetate (2): Chlorosulfonic acid (7.0 mL) was added dropwise to a solution of ethyl 2-phenoxyacetate (2 g, 11 mmol) in dichloromethane (50 mL) and cooled with ice. After stirring for 3 h at RT, the reaction mixture was poured into ice-cold water (20 mL) and extracted two times with diethyl ether (40 mL). The combined organic extracts were dried with anhydrous $MgSO_4$ and concentrated under reduced pressure to provide the sulfonyl chloride **2** as a yellowish oil (2.40 g, 78% yield). ^1H NMR ($CDCl_3$, 400 MHz): $\delta=1.32$ (t, $J=7.1$ Hz, 3H), 4.29 (q, $J=7.1$ Hz, 2H), 4.73 (s, 2H), 7.04 (d, $J=9.3$ Hz, 2H), 7.97 ppm (d, $J=9.3$ Hz, 1H); MS (70 eV): *m*/*z* (%): 278/280 (39/15) [M^+], 243 (100); EI-HRMS: *m*/*z* calcd (%) for [M^+] $C_{10}H_{11}ClO_5S$: 278.0016; found: 278.0049.

Ethyl [4-(2-formylphenylsulfamoyl)phenoxy]acetate (3): A mixture of **1** (500 mg, 4.06 mmol), **2** (1.4 g, 5.0 mmol), and pyridine (0.5 mL) in dichloromethane (5 mL) was stirred at RT for 2 h. The reaction mixture was quenched with water (50 mL) and extracted twice with dichloromethane. The combined organic extracts were dried with anhydrous $MgSO_4$ and concentrated under reduced pressure to give ethyl [4-(2-hydroxymethylphenylsulfamoyl)phenoxy]acetate as a yellow oil (1.42 g). Without further purification, the product was dissolved in dichloromethane (10 mL) and stirred together with manganese dioxide (4.8 g) at RT overnight. The suspension was filtered through a pad of Celite and concentrated under reduced pressure. Recrystallization from ethyl acetate provided aldehyde **3** as a white solid (783 mg, 53% yield). M.p. 83–85 °C; ^1H NMR ($CDCl_3$, 400 MHz): $\delta=1.27$ (t, $J=7.1$ Hz, 3H), 4.24 (q, $J=7.1$ Hz, 2H), 4.62 (s, 2H), 6.89 (d, $J=8.7$ Hz, 2H), 7.15 (t, $J=7.6$ Hz, 1H), 7.49 (t, $J=7.1$ Hz, 1H), 7.58 (dd, $J=7.4$, 1.4 Hz, 1H), 7.66 (d, $J=8.2$ Hz, 1H), 7.81 (d, $J=8.7$ Hz, 2H), 9.81 (s, 1H), 10.75 ppm (s, 1H); ^{13}C NMR ($CDCl_3$, 100 MHz): $\delta=14.6$, 62.0, 65.6, 115.1, 118.0, 122.1, 123.2, 129.7, 132.2, 136.0, 136.3, 140.0, 161.5, 167.9, 195.0 ppm; MS (70 eV): *m*/*z* (%): 363 (34) [M^+], 243 (35), 120 (100); EI-HRMS: *m*/*z* calcd for [M^+] $C_{17}H_{17}NO_6S$: 363.0776; found: 363.0771; elemental analysis calcd (%) for

$C_{17}H_{17}NO_6S$ (363.4): C 56.19, H 4.72, N 3.85; found: C 56.26, H 4.64, N 3.93.

Ethyl {4-[2-(4-formyl-1*H*-benzimidazol-2-yl)phenylsulfamoyl]phenoxy}-acetate (5): Acetic acid (0.280 mL), aldehyde **3** (1.11 g, 3.06 mmol) in MeOH (5 mL), and copper(II) acetate monohydrate (610 mg) in water (10 mL) were sequentially added with stirring to a solution of 2,3-diaminobenzyl alcohol **4** (300 mg, 2.17 mmol) in EtOH/H_2O (20 mL, 1:1). The mixture was heated under reflux for 3 h, filtered hot, and the residue washed with water. The precipitate was redissolved in a mixture of ethanol (12 mL) and concd HCl (2.2 mL). After addition of $Na_2S{\cdot}9H_2O$ (1.05 g in 8 mL water) the mixture was heated under reflux for 1 h, cooled to RT, and filtered through a pad of Celite to remove the precipitated CuS. The filtrate was neutralized with aqueous $NaHCO_3$ and extracted three times with dichloromethane. The combined organic extracts were dried with $MgSO_4$ and concentrated under reduced pressure. The crude product was purified on silica gel (hexanes/ethyl acetate 1:2→1:1) to provide the hydroxymethyl-substituted benzimidazole as a glassy, yellowish solid (378 mg, 36% yield). M.p. 54–56°C; ^{1}H NMR ($CDCl_3$, 400 MHz) (note: tautomeric proton exchange broadens a few signals): δ=1.30 (t, J=7.1 Hz, 3H), 4.26 (q, J=7.1 Hz, 2H), 4.50 (s, 2H), 5.02 (s, 2H), 6.39 (d, J=8.7 Hz, 2H), 7.09 (brs, 1H), 7.15 (t, J=7.6 Hz, 2H), 7.22 (d, J=7.6 Hz, 1H), 7.33 (brs, 1H), 7.32 (t, J=7.6 Hz, 2H), 7.49 (d, J=7.6 Hz, 1H), 7.67 (brs, 1H), 7.73 (d, J=7.6 Hz, 1H), 9.80 (brs, 1H), 9.99 ppm (brs, 1H); MS (70 eV): m/z (%): 481 (65) [M^+], 435 (27), 312 (31), 220 (100); EI-HRMS: m/z calcd (%) for [M^+] $C_{24}H_{23}N_3O_6S$: 481.1308; found: 481.1297.

The above intermediate (482 mg, 1.0 mmol) was dissolved in dichloromethane (15 mL) and stirred with manganese dioxide (1.1 g) at RT overnight. The suspension was filtered through a pad of Celite and concentrated under reduced pressure. Recrystallization from diethylether provided aldehyde **5** as a glassy, yellow solid (415 mg, 86% yield). M.p. 65–67°C; ^{1}H NMR ($CDCl_3$, 400 MHz): δ=1.24 (t, J=7.1 Hz, 3H), 4.21 (q, J=7.1 Hz, 2H), 4.52 (s, 2H), 6.65 (d, J=8.8 Hz, 2H), 7.17 (t, J=8.0 Hz, 1H), 7.39 (td, J=8.8, 1.7 Hz, 1H), 7.49 (t, J=8.0 Hz, 1H), 7.64 (d, J=9.3 Hz, 2H), 7.68 (dd, J=8.8, 1.1 Hz, 1H), 7.79 (dd, J=8.5, 1.7 Hz , 2H), 8.11 (d, J=7.7 Hz, 1H), 10.11 (s, 1H), 10.87 (brs, 1H), 12.35 ppm (s, 2H); ^{13}C NMR ($CDCl_3$, 100 MHz): δ=14.5, 61.9, 65.3, 114.5, 115.6, 116.4, 121.0, 121.3, 123.0, 123.8, 126.2, 126.9, 127.8, 129.3, 131.7, 132.2, 138.0, 149.0, 151.9, 160.9, 167.9, 192.4 ppm; MS (70 eV): m/z (%): 479 (64) [M^+], 415 (25), 378 (5), 328 (50), 236 (100), 209 (11), 181 (9); EI-HRMS: m/z calcd (%) for [M^+] $C_{24}H_{21}N_3O_6S$: 479.1151; found: 479.1145; elemental analysis calcd (%) for $C_{24}H_{21}N_3O_6S$ (479.5): C 60.12, H 4.41, N 8.76; found: C 60.24, H 4.49, N 8.66.

Ethyl {4-[2-(1*H*-benzimidazol-2-yl)phenylsulfamoyl]phenoxy}acetate (6a): A solution of 2-(2′-aminophenyl)benzimidazole (310 mg, 1.48 mmol) and **2** (500 mg, 1.79 mmol) in pyridine (3 mL) was stirred for 2 h. The reaction mixture was diluted with water (20 mL) and extracted twice with ethyl acetate (40 mL). The combined organic extracts were dried with $MgSO_4$ and concentrated under reduced pressure. The crude product was purified by flash chromatography on silica gel (hexanes/ethyl acetate 2:1) to give ligand **6a** as a yellowish solid (400 mg, 60% yield). M.p. 134–136°C; ^{1}H NMR ([D$_6$]DMSO, 400 MHz): δ=1.12 (t, J=6.6 Hz, 3H), 4.08 (q, J=7.1 Hz, 2H), 4.77 (s, 2H), 6.92 (d, J=8.8 Hz, 2H), 7.19 (t, J=7.7 Hz, 1H), 7.28–7.31 (m, 2H), 7.40 (t, J=7.7 Hz, 1H), 7.60 (d, J=8.8 Hz, 1H), 7.64–7.67 (m, 4H), 8.02 (d, J=8.2 Hz, 1H), 13.23 ppm (s, 2H); ^{13}C NMR ($CDCl_3$, 100 MHz): δ=14.8, 61.5, 65.4, 115.7, 116.4, 119.2, 123.8, 124.0, 128.0, 129.5, 131.5, 131.8, 151.0, 161.5, 168.5, 168.5 ppm; MS (70 eV): m/z (%): 451.1 (44) [M^+], 387.1 (14), 300.1 (40), 208.1 (100); EI-HRMS: m/z calcd (%) for [M^+] $C_{23}H_{21}N_3O_5S$: 451.1202; found: 451.1189; elemental analysis calcd (%) for $C_{23}H_{21}N_3O_5S$ (451.5): C 61.18, H 4.69, N 9.31; found: C 61.09, H 4.72, N 9.36.

{4-[2-(1*H*-Benzimidazol-2-yl)phenylsulfamoyl]phenoxy}acetic acid (6b): Ethyl ester **6a** (170 mg, 0.38 mmol) was added to a solution of LiOH·H_2O (350 mg) in a mixture of methanol (1 mL) and water (1 mL). The mixture was stirred at RT for 1 h, and the organic solvent subsequently removed under reduced pressure. The aqueous residue was acidified by the addition of 1 M HCl and the product then extracted twice with ethyl acetate. The combined organic extracts were dried with $MgSO_4$ and concentrated under reduced pressure to provide acid **6b** as a yellowish solid (140 mg, 88% yield). For the photophysical studies a sample of the compound (10 mg) was further purified by semipreparative reversed-phase HPLC (10×300 mm C18 column, CH_3CN/H_2O (0.01% TFA) 75:25→98:2); M.p. 140°C (decomp); ^{1}H NMR ([D$_6$]DMSO, 400 MHz): δ=4.66 (s, 2H), 6.90 (d, J=8.8 Hz, 2H), 7.19 (t, J=7.7 Hz, 1H), 7.28–7.31 (m, 2H), 7.40 (t, J=7.7 Hz, 1H), 7.60 (d, J=8.8 Hz, 1H), 7.65–7.67 (m, 4H), 8.02 (d, J=8.2 Hz, 1H), 13.23 ppm (s, 2H); MS (70 eV): m/z (%): 423 (20) [M^+], 300 (17), 208 (100); EI-HRMS: m/z calcd (%) for [M^+] $C_{21}H_{17}N_3O_5S$: 423.0889; found: 423.0863.

Ethyl {4-{2-{4-[(diethylamino)methyl]-1*H*-benzimidazol-2-yl}phenylsulfamoyl}phenoxy}acetate (7a): Diethyl amine (31 μL, 0.292 mmol) and sodium triacetoxyborohydride (66 mg, 0.313 mmol) were added to a solution of aldehyde **5** (100 mg, 0.209 mmol) in 1,2-dichloroethane (15 mL). The reaction mixture was allowed to stir for 2.5 h under N_2 and was then quenched by the addition of 1 M aqueous NH_4OH (3 mL). The product was extracted twice with dichloromethane and the combined organic extracts were dried with $MgSO_4$. The organic solvent was evaporated under reduced pressure and the residue purified by using flash chromatography on silica gel (dichloromethane/methanol/TFA 50:1:0.25→50:1:0.5) to provide ligand **7a** as a glassy, pale yellow solid (85 mg, 76% yield). M.p. 54–56°C; ^{1}H NMR ($CDCl_3$, 400 MHz): δ=1.15 (t, J=7.1 Hz, 3H), 1.23 (t, J=7.1 Hz, 6H), 2.68 (q, J=6.9 Hz, 4H), 4.01 (s, 2H), 4.20 (q, J=7.1 Hz, 2H), 4.52 (s, 2H), 6.70 (d, J=8.8 Hz, 2H), 7.08–7.13 (m, 2H), 7.20 (t, J=7.7 Hz, 1H), 7.30 (t, J=7.7 Hz, 1H), 7.30 (t, J=8.2 Hz, 1H), 7.63 (brs, 1H), 7.67 (d, J=7.7 Hz, 1H), 7.70–7.74 (m, 3H), 9.44 (brs, 1H), 12.52 ppm (brs, 1H); ^{13}C NMR ($CDCl_3$, 100 MHz): δ=8.1, 10.5, 43.2, 52.2, 57.9, 61.4, 110.6, 112.7, 114.6, 116.3, 118.9, 119.1, 119.6, 120.6, 122.3, 122.6, 125.4, 126.8, 128.6, 129.5, 134.0, 145.7, 156.8, 164.0 ppm; MS (70 eV): m/z (%): 536 (1) [M^+], 507 (52), 465 (100), 222 (100), 72 (25); EI-HRMS: m/z calcd (%) for [M^+] $C_{28}H_{32}N_4O_5S$: 536.2093; found: 536.2065; elemental analysis calcd (%) for $C_{28}H_{32}N_4O_5S{\cdot}0.5H_2O$ (545.7): C 61.63, H 6.10, N 10.27; found: C 61.83, H 6.13, N 9.93.

{4-{2-{4-[(Diethylamino)methyl]-1*H*-benzimidazol-2-yl}phenylsulfamoyl}-phenoxy}acetic acid (7b): Ethyl ester **7a** (22 mg, 0.041 mmol) was hydrolyzed as described for acid **6b** to provide the free acid **7b** (12 mg, 58%). M.p. 225–227°C; ^{1}H NMR (CD_3OD, 400 MHz): δ=1.42 (t, J=7.1 Hz, 6H), 3.35 (q, J=7.4 Hz, 4H), 3.63 (brs, 1H), 4.34 (s, 2H), 4.74 (s, 2H), 6.61 (d, J=8.2 Hz, 2H), 7.24 (t, J=7.4 Hz, 1H), 7.32 (d, J=7.7 Hz, 2H), 7.34–7.45 (m, 3H), 7.69 (t, J=6.9 Hz, 2H), 7.81 ppm (dd, J=8.7, 1.1 Hz, 1H); MS (70 eV): m/z (%): 509 (100) [M+1]$^+$, 435 (5), 338 (15), 295 (44); ESI-TOF-HRMS: m/z calcd (%) for [M+1]$^+$ $C_{26}H_{29}N_4O_5S$: 509.1859; found: 509.1884.

Ethyl {4-{2-{4-[(methylpyridin-2-ylmethylamino)methyl]-1*H*-benzimidazol-2-yl}phenylsulfamoyl}phenoxy}acetate (8a): Prepared as described for **7a** by reductive amination of aldehyde **5** (100 mg, 0.209 mmol) with methyl picolylamine[47] (100 mg, 0.819 mmol), providing **8a** as a glassy, pale yellow solid (119 mg, 97% yield). M.p. 56–58°C; ^{1}H NMR ($CDCl_3$, 400 MHz): δ=1.22 (t, J=7.1 Hz, 3H), 2.29 (s, 3H), 3.74 (s, 2H), 3.89 (s, 2H), 4.18 (q, J=7.1 Hz, 2H), 4.41 (s, 2H), 6.64 (m, 2H), 7.03 (d, J=7.1 Hz, 1H), 7.14–7.18 (m, 3H), 7.27 (d, J=7.7 Hz, 1H), 7.33 (td, J=7.7, 1.7 Hz, 1H), 7.65 (dd, J=7.7, 2.2 Hz, 1H), 7.68–7.73 (m, 3H), 7.78 (dd, J=8.2, 1.1 Hz, 1H), 8.18 (d, J=7.7 Hz, 1H), 8.43 (d, J=4.4 Hz, 1H), 13.48 ppm (brs, 2H); ^{13}C NMR ($CDCl_3$, 100 MHz): δ=14.4, 43.0, 58.8, 61.8, 63.1, 65.3, 114.5, 117.6, 118.2, 120.3, 122.1, 122.5, 122.8, 123.4, 123.6, 123.9, 127.2, 129.4, 130.5, 132.8, 133.1, 137.3, 138.0, 143.0, 149.2, 150.5, 159.0, 160.6, 167.9 ppm; MS (70 eV): m/z (%): 586 (100) [M+1]$^+$, 344 (13), 293 (27); ESI-TOF-HRMS: m/z calcd (%) for [M+1]$^+$ $C_{31}H_{32}N_5O_5S$: 586.2124; found: 586.2089; elemental analysis calcd (%) for $C_{31}H_{31}N_5O_5S$ (585.7): C 63.57, H 5.34, N 11.96; found: C 63.57, H 5.44, N 11.78.

{4-{2-{4-[(Methylpyridin-2-ylmethylamino)methyl]-1*H*-benzimidazol-2-yl}phenylsulfamoyl}phenoxy}acetic acid (8b): Ethyl ester **8a** (40 mg, 0.068 mmol) was hydrolyzed as described for acid **6b** to give free acid **8b** (23 mg, 61%). M.p. 133–135°C; ^{1}H NMR ($CDCl_3$, 400 MHz): δ=2.47 (s, 3H), 3.63 (brs, 1H), 4.08 (s, 2H), 4.22 (s, 2H), 4.36 (s, 2H), 6.40 (d, J=8.3 Hz, 2H), 7.06–7.18 (m, 4H), 7.28 (d, J=6.1 Hz, 2H), 7.31 (d, J=7.7 Hz, 4H), 7.69 (d, J=6.7 Hz, 2H), 7.75 (d, J=7.1 Hz, 2H), 8.55 ppm (d, J=4.4 Hz, 1H); MS (70 eV): m/z (%): 558 (100) [M+1]$^+$, 344 (5), 279, (19); ESI-TOF-HRMS: m/z calcd (%) for [M+1]$^+$ $C_{29}H_{28}N_5O_5S$: 558.1811; found: 558.1846.

Ethyl {4-{2-{4-[(bispyridin-2-ylmethylamino)methyl]-1*H*-benzimidazol-2-yl}phenylsulfamoyl}phenoxy}acetate (9a): Prepared as described for **7a**

by reductive amination of aldehyde **5** (40 mg, 0.083 mmol) with 2,2′-dipicolylamine (22 mg, 0.11 mmol), providing **9a** as a glassy solid (44 mg, 80% yield). M.p. 65–67 °C; ^{1}H NMR ($CDCl_3$, 400 MHz): $\delta = 1.23$ (t, $J =$ 7.1 Hz, 3H), 3.89 (s, 2H), 3.91 (s, 4H), 4.19 (q, $J = 7.1$ Hz, 2H), 4.41 (s, 2H), 6.66 (d, $J = 9.3$ Hz, 2H), 7.09–7.20 (m, 4H), 7.25 (d, $J = 7.6$ Hz, 2H), 7.36 (td, $J = 8.5$, 1.4 Hz, 1H), 7.54 (td, $J = 7.6$, 1.6 Hz, 2H), 7.72–7.77 (m, 3H), 7.81 (dd, $J = 8.2$, 1.1 Hz, 1H), 8.17 (dd, $J = 7.9$, 1.1 Hz, 1H), 8.40 (d, $J = 3.8$ Hz, 2H), 13.20 (br s, 2H), 14.11 ppm (s, 1H); ^{13}C NMR ($CDCl_3$, 400 MHz): $\delta = 14.5$, 56.5, 59.9, 61.9, 65.4, 114.6, 118.6, 120.6, 122.3, 122.6, 123.0, 123.3, 123.6, 123.7, 126.9, 129.5, 130.6, 133.0, 133.3, 137.1, 138.1, 143.0, 149.0, 150.6, 159.2, 160.7, 167.9 ppm; MS (70 eV): m/z (%): 662 (5) [M^+], 570 (100), 465 (13), 222 (40), 198 (53), 93 (78); EI-HRMS: m/z calcd (%) for [M^+] $C_{36}H_{34}N_6O_5S$: 662.2311; found: 662.2276; elemental analysis calcd (%) for $C_{36}H_{34}N_6O_5S \cdot 0.5\,H_2O$ (671.8): C 64.37, H 5.25, N 12.51; found: C 64.76, H 5.13, N 12.16.

{4-{2-{4-[(Bispyridin-2-ylmethylamino)methyl]-1*H*-benzimidazol-2-yl}-phenylsulfamoyl}phenoxy}acetic acid (9b): Ethyl ester **9a** (22 mg, 0.033 mmol) was hydrolyzed as described for acid **6b** to give free acid **9b** (16 mg, 76%). For all photophysical studies a sample of the compound (10 mg) was further purified by semipreparative reversed-phase HPLC (10×300 mm C18 column, CH_3CN/H_2O (0.01% TFA) 75:25→98:2). M.p. 80–82 °C; ^{1}H NMR ($CDCl_3$, 400 MHz): $\delta = 3.91$ (s, 4H), 3.99 (s, 2H), 4.39 (s, 2H), 6.50 (d, $J = 8.7$ Hz, 2H), 7.06 (d, $J = 7.1$ Hz, 1H), 7.16 (t, $J =$ 7.6 Hz, 4H), 7.25 (s, 2H), 7.38 (t, $J = 7.6$ Hz, 1H), 7.52 (d, $J = 8.7$ Hz, 2H), 7.59 (td, $J = 7.6$, 1.4 Hz, 2H), 7.68 (d, $J = 7.6$ Hz, 1H), 7.83 (d, $J =$ 8.2 Hz, 1H), 8.00 (d, $J = 7.6$ Hz, 1H), 8.40 ppm (d, $J = 4.9$ Hz, 2H); FAB-MS (thioglycerol): m/z (%): 635 (100) [M^+], 373 (62); FAB-HRMS: m/z calcd (%) for [M+H]$^+$ $C_{34}H_{31}N_6O_5S$: 635.2077; found: 635.2119.

Steady-state absorption and fluorescence spectroscopy: All sample stock solutions and buffer solutions were filtered through 0.2 μm Nylon membrane filters to remove interfering dust particles or fibers. UV/Vis absorption spectra were recorded at 25 °C by using a Varian Cary Bio50 UV/Vis spectrometer with constant-temperature accessory. Steady-state emission and excitation spectra were recorded with a PTI fluorimeter and FELIX software. Throughout the titration the sample solution was stirred with a magnetic stirring device. For all titrations the path length was 1 cm with a cell volume of 3.0 mL. All fluorescence spectra have been corrected for the spectral response of the detection system (emission correction file provided by the instrument manufacturer) and for the spectral irradiance of the excitation channel (by using a calibrated photodiode). Quantum yields were determined by using quinine sulfate dihydrate in 1.0 N H_2SO_4 ($\Phi_f = 0.543 \pm 0.03$) as the fluorescence standard.[48]

Electrode calibration in aqueous solution: Measurements were performed with an Orion microcombination glass electrode. The electrode was calibrated for $-\log[H_3O^+]$ by titration of a standardized HCl solution (Aldrich, 0.1 N volumetric standard) with KOH (Aldrich, 0.1 N volumetric standard) at 25 °C and 0.1 M ionic strength (KCl). The endpoint, electrode potential, and slope were determined by using Gran's method[34] as implemented in the software GLEE.[49] The calibration procedure was repeated three times prior to each pK_a value determination. The electrode potential was measured with the Corning pH/Ion Analyzer 355 and the emf measurements were reproducible with ±0.1 mV accuracy.

Potentiometry: All protonation constants reported in this study were determined from potentiometric titrations and additionally confirmed by spectrophotomotetric measurements. Potentiometric titrations were carried out with a motorized burette (Dosimat, Metrohm, Switzerland) by adding a total of 40–100 aliquots of KOH (0.1 M) to 10.0 mL of a solution of the corresponding ligand (0.5–1.0 mM) in KCl (0.1 M) under a N_2 atmosphere (solvent-vapor-saturated gas). Throughout the titration, the temperature was maintained at 25 ± 0.1 °C by circulating constant-temperature water through the water-jacket of the titration cell. For the potentiometric titration of ligands **7b**, **8b**, and **9b**, the initial solution was further acidified by adding 1–3 molar equivalents of HCl (0.5 M). The emf data were converted to $-\log[H_3O^+]$ based on the electrode potential $E°$ and slope, which were determined as described above prior to each titration. The pK_a values were obtained from nonlinear least-squares fit analysis of the potentiometric data.[35]

Spectrophotometric titrations: The UV/Vis absorption spectra of the ligands were monitored for a series of solutions in which $-\log[H_3O^+]$ was varied between 5 and 11. The emf of each solution was directly measured in the UV quartz cell (electrode diameter 3 mm) and converted to $-\log[H_3O^+]$ using the $E°$ and slope, as obtained from the electrode calibration procedure described above. The raw spectral and emf data were processed with nonlinear least-squares fit analysis using the SPECFIT software package.[38]

Complex stability constants: All reported stability constants K were measured at pH 7.2 (PIPES 10 mM, 0.1 M $KClO_4$ ionic background) and refer to apparent stability constants.[50]

*Determination of the apparent Zn^{II} affinity of ligands **6b** and **7b***: UV/Vis spectrophotometric titrations were performed with a 60 μM solution (3.0 mL cell volume) of the corresponding ligand in PIPES buffer (10 mM, pH 7.20, 0.1 M $KClO_4$) over the range of 4 logarithmic units of free Zn^{II}. The recorded spectra were processed by nonlinear least-squares fit analysis using the SPECFIT software package.[38] The resulting binding affinities are apparent stability constants, and are defined by Equation (2):

$$K' = \frac{[ZnL]}{[Zn]([L] + [LH] + [LH_2] + \ldots [LH_m])} \quad (2)$$

in which [ZnL] = concentration of zinc–ligand complex, [Zn] = concentration of unbound Zn^{II}, ([L] + [LH] + … [LH_m]) = concentration of all ligand species that do not involve Zn^{II} (at given conditions of pH 7.2, 0.1 M $KClO_4$, 25 °C).[50]

*Determination of the apparent Zn^{II} affinity of ligand **8b** and **9b***: A series of PIPES-buffered solutions (10 mM, pH 7.20, 0.1 M $KClO_4$) were prepared that contained HEDTA (10 mM) or EGTA (10 mM) and between 1–9 mM of $Zn(OTf)_2$. The concentration of free Zn^{II} was calculated using the program Hyss,[51] based on the following published pK_a and log K values for HEDTA, p$K_1 = 9.87$, p$K_2 = 5.38$, p$K_3 = 2.62$, p$K_4 = 1.60$, log K(ZnL) = 14.6 (25 °C, $\mu = 0.1$), and EGTA, p$K_1 = 9.40$, p$K_2 = 8.79$, p$K_3 = 2.70$, log K(ZnL) = 12.6 (25 °C, $\mu = 0.1$).[41] According to Martell and Smith,[41] the tabulated pK_a data must be corrected upward by 0.11 to account for 0.1 M ionic strength. This correction is necessary because the tabulated pK_a values are determined on the basis of the concentration and not the activity of the hydronium ions. For the calculation of the free Zn^{II} concentrations, the published pK_a values of HEDTA and EGTA were therefore corrected by 0.11. Ligands **8b** or **9b** were dissolved in 3.0 mL of the corresponding buffer solutions up to a final concentration of 10 μM. After a 24 h equilibration time, the fluorescence intensity at 400 and 500 nm was determined. The experimental data were analyzed by a nonlinear least-squares fit algorithm with the following formalisms:

By assuming a 1:1 metal-to-ligand stoichiometry, the following relationship [Eq. (3)] was found between the free Zn^{II} concentration, apparent dissociation constant K_d, and fluorescence intensity F:[4]

$$[Zn] = K_d \frac{F - F_{min}}{F_{max} - F} \quad (3)$$

in which F_{min} = fluorescence intensity of free ligand, F_{max} = fluorescence intensity of Zn^{II}-bound ligand.

Using Equation (3) the emission intensity F can be expressed as a function of free Zn^{II} and K_d, as shown in Equation (4):

$$F = \frac{[Zn]F_{max} + K_d F_{min}}{K_d + [Zn]} \quad (4)$$

Nonlinear least-squares fit analysis of the experimental intensities versus the (calcd) free Zn^{II} concentrations allowed for the determination of F_{max}, F_{min}, and K_d.

Acknowledgements

Financial support from the Georgia Institute of Technology is gratefully acknowledged. We also thank D. Bostwick for mass spectral data, and J. Cody for a critical review of the manuscript.

[1] A. P. DeSilva, H. Q. N. Gunaratne, T. Gunnlaugsson, A. J. M. Huxley, C. P. McCoy, J. T. Rademacher, T. E. Rice, *Chem. Rev.* **1997**, *97*, 1515.
[2] W. T. Mason, *Fluorescent and Luminescent Probes for Biological Activity*, Academic Press, San Diego, **1999**.
[3] K. Rurack, *Spectrochim. Acta Part A* **2001**, *57*, 2161.
[4] G. Grynkiewicz, M. Poenie, R. Y. Tsien, *J. Biol. Chem.* **1985**, *260*, 3440.
[5] R. Y. Tsien, *Trends Neurosci.* **1988**, *11*, 419.
[6] R. P. Haugland, *Handbook of Fluorescent Probes and Research Products*, Molecular Probes, Eugene, Oregon, **2002**.
[7] P. D. Zalewski, S. H. Millard, I. J. Forbes, O. Kapaniris, A. Slavotinek, W. H. Betts, A. D. Ward, S. F. Lincoln, I. Mahadevan, *J. Histochem. Cytochem.* **1994**, *42*, 877.
[8] R. D. Palmiter, T. B. Cole, S. D. Findley, *EMBO J.* **1996**, *15*, 1784.
[9] R. D. Palmiter, T. B. Cole, C. J. Quaife, S. D. Findley, *Proc. Natl. Acad. Sci. USA* **1996**, *93*, 14934.
[10] T. Budde, A. Minta, J. A. White, A. R. Kay, *Neuroscience* **1997**, *79*, 347.
[11] H. J. Wenzel, T. B. Cole, D. E. Born, P. A. Schwartzkroin, R. D. Palmiter, *Proc. Natl. Acad. Sci. USA* **1997**, *94*, 12676.
[12] M. S. Nasir, C. J. Fahrni, D. A. Suhy, K. J. Kolodsick, C. P. Singer, T. V. O'Halloran, *J. Biol. Inorg. Chem.* **1999**, *4*, 775.
[13] C. W. MacDiarmid, L. A. Gaither, D. Eide, *EMBO J.* **2000**, *19*, 2845.
[14] G. Ranaldi, G. Perozzi, A. Truong-Tran, P. Zalewski, C. Murgia, *Am. J. Physiol.* **2002**, *283*, 1365.
[15] H. Haase, D. Beyersmann, *Biochem. Biophys. Res. Commun.* **2002**, *296*, 923.
[16] C. P. Kirschke, L. P. Huang, *J. Biol. Chem.* **2003**, *278*, 4096.
[17] S. C. Burdette, C. J. Frederickson, W. Bu, S. J. Lippard, *J. Am. Chem. Soc.* **2003**, *125*, 1778.
[18] T. Hirano, K. Kikuchi, Y. Urano, T. Nagano, *J. Am. Chem. Soc.* **2002**, *124*, 6555.
[19] K. R. Gee, Z. L. Zhou, W. J. Qian, R. Kennedy, *J. Am. Chem. Soc.* **2002**, *124*, 776.
[20] E. Kimura, S. Aoki, E. Kikuta, T. Koike, *Proc. Natl. Acad. Sci. USA* **2003**, *100*, 3731.
[21] D. A. Pearce, N. Jotterand, I. S. Carrico, B. Imperiali, *J. Am. Chem. Soc.* **2001**, *123*, 5160.
[22] C. J. Fahrni, T. V. O'Halloran, *J. Am. Chem. Soc.* **1999**, *121*, 11448.
[23] K. R. Gee, Z. L. Zhou, D. Ton-That, S. L. Sensi, J. H. Weiss, *Cell Calcium* **2002**, *31*, 245.
[24] S. Maruyama, K. Kikuchi, T. Hirano, Y. Urano, T. Nagano, *J. Am. Chem. Soc.* **2002**, *124*, 10650.
[25] M. M. Henary, C. J. Fahrni, *J. Phys. Chem. A* **2002**, *106*, 5210.
[26] K. Das, N. Sarkar, D. Majumdar, K. Bhattacharyya, *Chem. Phys. Lett.* **1992**, *198*, 443.
[27] H. K. Sinha, S. K. Dogra, *Chem. Phys.* **1986**, *102*, 337.
[28] M. Mosquera, J. C. Penedo, M. C. Rios Rodriguez, F. Rodriguez-Prieto, *J. Phys. Chem.* **1996**, *100*, 5398.
[29] S. Santra, G. Krishnamoorthy, S. K. Dogra, *J. Phys. Chem. A* **2000**, *104*, 476.
[30] S. Santra, S. K. Dogra, *Chem. Phys.* **1998**, *226*, 285.
[31] C. J. Fahrni, M. M. Henary, D. G. VanDerveer, *J. Phys. Chem. A* **2002**, *106*, 7655.
[32] M. Bonnat, M. Bradley, J. D. Kolburn, *Tetrahedron Lett.* **1996**, *37*, 5409.
[33] W. H. Kwok, H. Zhang, P. Payra, M. Duan, S.-C. Hung, D. H. Johnston, J. Gallucci, E. Skrzypczak-Jankun, M. K. Chan, *Inorg. Chem.* **2000**, *39*, 2367.
[34] G. Gran, *Analyst* **1951**, *77*, 661.
[35] A. E. Martell, R. J. Motekaitis, *The Determination and Use of Stability Constants*, VCH, New York, **1992**.
[36] J. K. Romary, J. D. Barger, J. E. Bunds, *Inorg. Chem.* **1968**, *7*, 1142.
[37] D. W. Gruenwedel, *Inorg. Chem.* **1968**, *7*, 495.
[38] R. A. Binstead, A. D. Zuberbühler, SPECFIT Global Analysis System, Spectrum Software Associates, Marlborough MA 01752, **2001**.
[39] V. I. Minkin, A. D. Garnovskii, J. Elguero, A. R. Katritzky, O. V. Denisko, *Adv. Heterocycl. Chem.* **2000**, *76*, 157.
[40] J. Elguero, C. Marzin, A. R. Katritzky, P. Linda, *Adv. Heterocycl. Chem., Suppl. 1*, **1976**.
[41] A. E. Martell, R. M. Smith, NIST Critical Stability Constants of Metal Complexes, NIST Standard Reference Database 46, Version 5.0, **1998**.
[42] D. A. Deranleau, *J. Am. Chem. Soc.* **1969**, *91*, 4044.
[43] J. E. Coleman, K. Nakamura, J. F. Chlebowski, *J. Biol. Chem.* **1983**, *258*, 386.
[44] J. E. Coleman, B. L. Vallee, *J. Biol. Chem.* **1960**, *235*, 390.
[45] J. A. Hunt, C. A. Fierke, *J. Biol. Chem.* **1997**, *272*, 20364.
[46] P. Canonne, M. Belley, G. Fytas, J. Plamondon, *Can. J. Chem.* **1988**, *66*, 168.
[47] U. Holzgrabe, *Arch. Pharm.* **1987**, *320*, 647.
[48] J. N. Demas, G. A. Crosby, *J. Phys. Chem.* **1971**, *75*, 991.
[49] P. Gans, B. O'Sullivan, *Talanta* **2000**, *51*, 33.
[50] G. Schwarzenbach, *Complexometric Titrations*, Interscience, New York, **1957**.
[51] L. Alderighi, P. Gans, A. Ienco, D. Peters, A. Sabatini, A. Vacca, *Coord. Chem. Rev.* **1999**, *184*, 311.
[52] Note added in proof: The following two reports on emission-ratiometric zinc-selective fluorescent sensors just appeared in print: M. Taki, J. L. Wolford, T. V. O'Halloran, *J. Am. Chem. Soc.* **2004**, *126*, 712 and C. J. Chang, J. Jaworski, E. M. Nolan, M. Sheng, S. J. Lippard, *Proc. Nat. Acad. Sci.* **2004**, *101*, 1129.

Received: July 3, 2003
Revised: December 24, 2003

Published online: April 28, 2004

